

Synthesis of Tetrahydrobenzo[*b*]pyran and Pyrano[2, 3-*d*]pyrimidinone Derivatives Using Fe₃O₄@Ph-PMO-NaHSO₄ as a New Magnetically Separable Nanocatalyst

Mahdiah Haghighat¹, Farhad Shirini^{1,*}, and Mostafa Golshekan²

¹Department of Chemistry, College of Sciences, University of Guilan, Rasht, 41335-19141, Iran

²Institute of Medical Advanced Technologies, Guilan University of Medical Science, Rasht, 41346-45971, Iran

Immobilized NaHSO₄ on core/shell phenylene bridged periodic mesoporous organosilica magnetic nanoparticles (Fe₃O₄@Ph-PMO-NaHSO₄) as a new acidic magnetically separable nanocatalyst was successfully prepared in three steps: (i) preparation of Fe₃O₄ nanoparticles by a precipitation method, (ii) synthesis of an organic-inorganic periodic mesoporous organosilica structure with phenyl groups on the surface of Fe₃O₄ magnetic nanoparticles (MNPs) and (iii) finally adsorption of NaHSO₄ on periodic mesoporous organosilica (PMO) network. The prepared organic-inorganic magnetic reagent was characterized by Fourier transform infrared spectroscopy (FT-IR), X-ray powder diffraction (XRD), transmission electron microscopy (TEM), N₂ adsorption-desorption and energy-dispersive X-ray (EDX) techniques. Finally, it was used as a reusable and new catalyst to promote the synthesis of tetrahydrobenzo[*b*]pyran and pyrano[2,3-*d*]pyrimidinone derivatives as important biologically active compounds. Eco-friendly protocol, high yields, short reaction times and easy and quick isolation of the products are the main advantages of this procedure.

Keywords: PMO, Nanocatalyst, Tetrahydrobenzo[*b*]pyran, Pyrano[2,3-*d*]pyrimidinone, Fe₃O₄@Ph-PMO-NaHSO₄.

1. INTRODUCTION

In recent years, porous materials have played a very important role in science and industry so that billion dollars are spent annually in the use of these materials in various fields. Some of these important fields are ionic exchange, separation, catalysis, preparation of batteries, fuel cells, sensors and many others. Among these materials, mesoporous silica has attracted considerable attention in the field of adsorption and catalysis because of its uniform pore size, large pore volume, and high surface area.¹ The surface of mesoporous silica can be modified with various types of organic functional groups, producing organic-inorganic hybrid materials, in order to use as a catalyst. Some members of these mesoporous materials such as MCM-41 and SBA-15 in spite of mentioned properties often suffer from pore blocking and in homogeneous distribution of the functional groups in

post-synthetic grafting method²⁻⁴ and remarkable decrease in the mesostructured arrangement and textural properties at a high loading level of functional groups.⁵⁻⁶ In 1999, use of periodic mesoporous organosilica materials as another member of this family has attracted the attention of research groups.⁷⁻⁹ Periodic mesoporous organosilica materials are a class of hybrid materials which in them organic groups are distributed uniformly inside the framework, causing properties including mechanical and hydrothermal stability, diffusion of guest molecule and lack of pore blocking and they are more hydrophobic and stable in water than pure organized silicas (MCM-41 or SBA-15). This feature expands the range of applications in, for example, optical gas sensing, catalysis, chromatography, separation and nanotechnology.¹⁰⁻¹² For the preparation of this kind of materials, a common method including hydrolysis and condensation of a bridged organosilane precursor of the type (R'O)₃Si-R-Si(OR')₃ (R' is methyl or ethyl and R is an organic group) in the presence of a structure directing agent can be used.

*Author to whom correspondence should be addressed.

On the other hand, the synthesis of catalysts based on the principles of green chemistry is very important and it will be possible by the preparation of nanocatalysts based on high selectivity and activity and easy separation. Simultaneous use of magnetic nanoparticles because of their easy separation and periodic mesoporous materials with their unique properties in a single material can be considered to follow the green chemistry principles.

The synthesis of natural molecules, pharmaceuticals and biologically active compounds for a long time has been a significant branch of organic synthesis. Tetrahydrobenzo[*b*]pyran and pyrano[2,3-*d*]pyrimidinones derivatives belong to important classes of nitrogen-containing heterocyclic compounds that show significant pharmaceutical and biological activities including anticancer, antitumor, antimalarial, antibacterial, antihypertensive, anti-inflammatory, hepatoprotective, cardiogenic, vasodilator, bronchodilator, antifolate, and antiallergic activities.^{13–19} Several synthetic methods have been reported to obtain more potentially biological derivatives of these compounds using catalysts such as *N*-methylimidazole,²⁰ tetrabutylammonium bromide,²¹ trisodium citrate,²² *p*-dodecylbenzenesulfonic acid,²³ poly(4-vinylpyridine),²⁴ potassium phthalimide-*N*-oxyl,²⁵ $\text{NH}_4\text{H}_2\text{PO}_4/\text{Al}_2\text{O}_3$,²⁶ $\text{Na}_2\text{CaP}_2\text{O}_7$,²⁷ $\text{NiFe}_2\text{O}_4 @ \text{SiO}_2 @ \text{H}_{14}[\text{NaP}_5\text{W}_{30}\text{O}_{110}]$ ²⁸ and silica coated magnetic NiFe_2O_4 nanoparticles supported $\text{H}_3\text{PW}_{12}\text{O}_{40}$ (NFS-PWA) (for the synthesis of tetrahydrobenzo[*b*]pyrans),²⁹ diammonium hydrogen phosphate,³⁰ *L*-proline,³¹ $\text{KAl}(\text{SO}_4)_2 \cdot 12\text{H}_2\text{O}$ (alum),³² tetrabutylammonium bromide,²¹ sulfonic acid nanoporous silica (SBA-Pr- SO_3H),³³ nano-sawdust- OSO_3H ,³⁴ Al-HMS-20,³⁵ and ZnO-supported copper oxide (for the synthesis of pyrano[2,3-*d*]pyrimidinones).³⁶ Despite undeniable advantages of these methods, most of them are accompanied with limitations including drastic reaction conditions,³³ difficulties in the preparation of the catalyst,³⁴ long reaction times³⁵ and non-recoverability of the catalyst. To overcome the drawbacks of these methods there has been continuous interest to develop easier methods for the synthesis of tetrahydrobenzo[*b*]pyran and pyrano[2,3-*d*]pyrimidinones derivatives. In the present study and in order to develop simple, efficient, and mild procedures using easily separable and reusable solid catalysts, a new magnetically separable solid acid nanocatalyst is prepared and applied to the synthesis of tetrahydrobenzo[*b*]pyrans and pyrano[2,3-*d*]pyrimidinones. This strategy involves Fe_3O_4 nanoparticles as the magnetic core coated by Ph-PMO as a thin layer on which NaHSO_4 is adsorbed.

2. EXPERIMENTAL DETAILS

2.1. Material

All chemicals including $\text{FeCl}_3 \cdot 6\text{H}_2\text{O}$, $\text{FeCl}_2 \cdot 4\text{H}_2\text{O}$, tetraethylorthosilicate (TEOS), 1,4-bis(triethoxysilyl)

benzene, sodium bisulfate monohydrate, Pluronic P-123 (M_n : $5800 \text{ g} \cdot \text{mol}^{-1}$), NaOH, benzaldehyde derivatives, 1,3-cyclohexanedione, barbituric acid, thiobarbituric acid and malononitrile were purchased with high purity from Sigma, Aldrich and Merck Companies. The purity determination of the substrate and reaction monitoring were accomplished by TLC on silica-gel polygram SILG/UV 254 plates.

2.2. Characterization Techniques

The crystallinity of the synthesized MNPs were analyzed by an X-PERT High Score X-ray diffraction (PANalytical) and measured with Cu $K\alpha$ radiations in the range of 0.78 – 80° (2θ). The quality and composition of the synthesized nanoparticles were characterized by a Perkin-Elmer spectrum BX series in the range of 400 – 4000 cm^{-1} . The size and morphology of particles were studied by a Philips transmission electron microscopy (TEM, CM10 HT 100 kV). Melting points were measured by a Büchi B-545 apparatus in open capillary tubes. N_2 adsorption-desorption was measured by a BELSORP-mini II instrument at 77 K. Before using the samples were degassed for 2 h at 120°C . The specific surface area of each material was calculated using the Brunauer–Emmett–Teller (BET) method. The EDX characterization of the catalyst was performed on a field emission scanning electron microscope making by TE-SCAN Company and equipped with energy dispersive X-ray spectrometer operating at 15 kV.

2.3. Preparation of Fe_3O_4 -MNPs

Fe_3O_4 -MNPs were chemically synthesized with a little modification in the methodology already described in the literature.³⁷ For the synthesis of Fe_3O_4 -MNPs, ferric chloride hexahydrate $\text{FeCl}_3 \cdot 6\text{H}_2\text{O}$ (11.0 g, 40.7 mmol) and ferrous chloride tetrahydrate $\text{FeCl}_2 \cdot 4\text{H}_2\text{O}$ (4.0 g, 20.1 mmol) were dissolved in deionized water (250 mL) under nitrogen atmosphere with mechanical stirrer at 85°C in order to prepare the stock solution of ferrous and ferric chloride. Then the prepared solution was slowly added to 250 mL of a 2 mol L^{-1} ammonia solution heated at 80°C under argon gas protection and vigorous stirring. During the process, the solution temperature was kept constant at 80°C and argon gas was purged to prevent the intrusion of oxygen. After completion of the reaction, the obtained precipitate of Fe_3O_4 -MNPs was separated from the reaction medium by the magnetic field and then was washed four times with 500 mL double-distilled water. Finally, the obtained Fe_3O_4 -MNPs were suspended in 500 mL of degassed deionized water.

2.4. Preparation of $\text{Fe}_3\text{O}_4 @ \text{Ph-PMO}$ Nanocomposite

For the synthesis of $\text{Fe}_3\text{O}_4 @ \text{Ph-PMO}$, 3.3 g Pluronic p123 ($M_n = 5800 \text{ g/mol}$) was dissolved in a mixture of Fe_3O_4 -MNPs (2 g) and concentrated HCl (0.55 mL) in distilled

water (120 mL) under argon gas protection at room temperature. Then, 1,4-bis(triethoxysilyl) benzene (2.3 mL) and tetraethoxysilane (1.5 mL) were added simultaneously to the mixture dropwise and stirred for 2 hours at 40 °C. At the end of this process, the magnetic composite was kept at 100 °C for 24 h under static conditions. The resultant solid was filtered, and the template was removed by solvent extraction. For this purpose, the magnetic nanocomposite was dispersed in acetone and refluxed at 56 °C for 10 h, then washed with distilled water and hot ethanol. This procedure was repeated twice to be sure of removing of the surfactant.

2.5. Preparation of Fe₃O₄@Ph-PMO-NaHSO₄ Nanocatalyst

Based on the method of Golshekan et al.,³⁹ Fe₃O₄@Ph-PMO-NaHSO₄ was prepared by adding the synthesized mesoporous Fe₃O₄@Ph-PMO nanoparticles (1.5 g) to an aqueous solution of NaHSO₄·H₂O (20 mL, 0.7 g, 5 mmol) and the mixture was sonicated at 25 °C for 1 min. In continue, the mixture was stirred for 30 min. Finally, water was removed by decanting and the powder was dried in an oven at 90 °C for 2 h. A brown solid acid formulated as Fe₃O₄@ph-PMO-NaHSO₄ was obtained. Schematic preparation of Fe₃O₄@ph-PMO-NaHSO₄ is shown in Figure 1.

2.6. General Procedure for the Synthesis of Tetrahydrobenzo[*b*]pyran Derivatives

A mixture of an aromatic aldehyde (1 mmol), malononitrile (1 mmol), dimedone (1.0 mmol), and

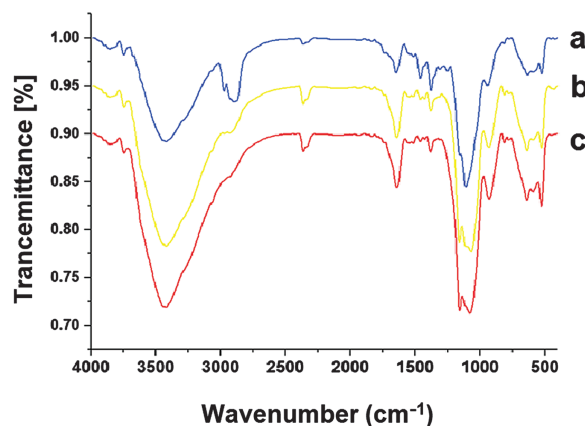


Figure 2. The FT-IR spectra of Fe₃O₄@Ph-PMO, before removal of the template (a), Fe₃O₄@Ph-PMO, after removal of the template (b) and Fe₃O₄@Ph-PMO-NaHSO₄ (c).

Fe₃O₄@Ph-PMO-NaHSO₄ (20 mg) in 3 mL aqueous ethanol (1:1) was stirred while heating at 80 °C in certain times. The reaction products were monitored using thin-layer chromatography (*n*-hexane:ethylacetate; 7:3). After completion of the reaction, the mixture was triturated with ethanol (3 mL). The magnetic nanocomposite was then separated in the presence of a magnetic stirring bar; the reaction mixture became clear. The crude product was recrystallized from ethanol to give the pure product.

2.7. General Procedure for the Synthesis of Pyrano[2,3-*d*]pyrimidinone Derivatives

Fe₃O₄@Ph-PMO-NaHSO₄ (30 mg) was added to a mixture of aromatic aldehyde (1 mmol), malononitrile

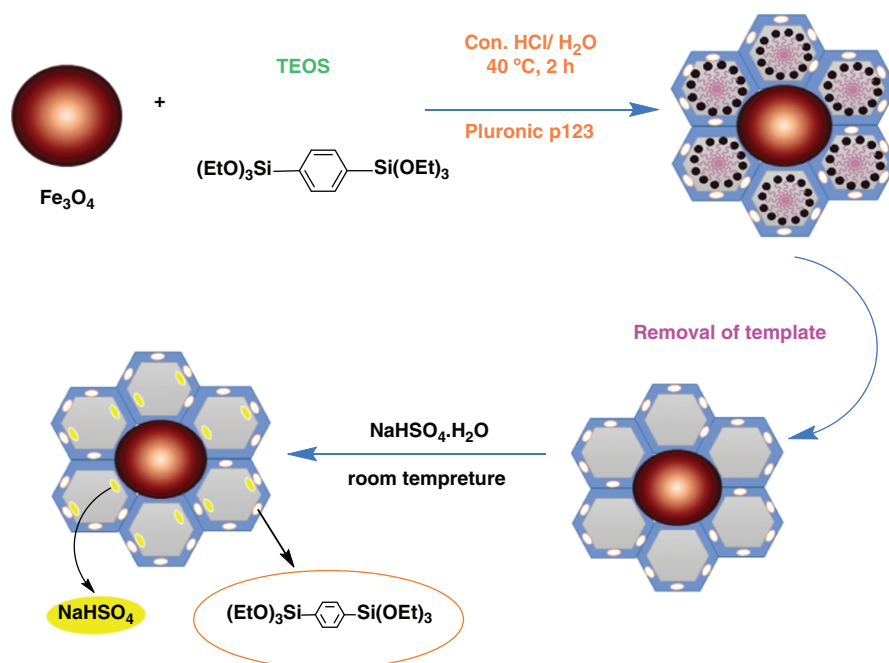


Figure 1. Preparation of Fe₃O₄@Ph-PMO-NaHSO₄.

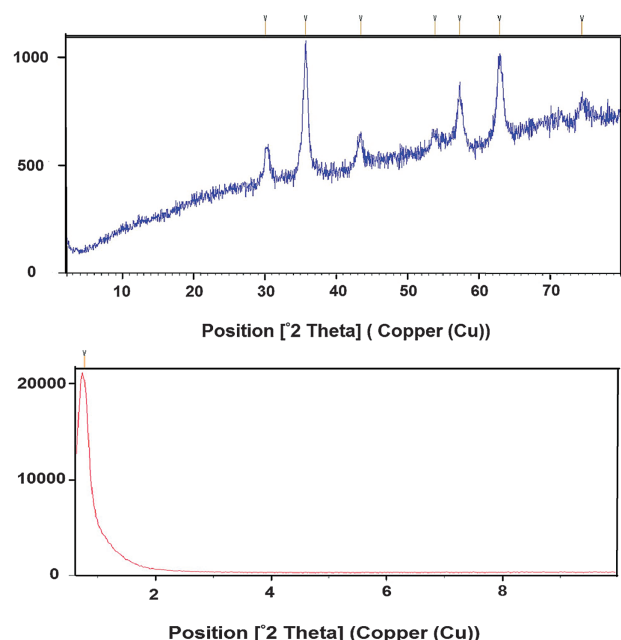


Figure 3. The XRD spectra of Fe_3O_4 @Ph-PMO after removal of the template.

(1 mmol) and barbituric or thiobarbituric acid (1 mmol) in water (3 mL). Then the mixture was heated at 80 °C in appropriate times and the progress of the reaction was indicated by TLC (*n*-hexane:ethyl acetate; 3:7). With completing the reaction, 3 ml ethanol was poured and the magnetic nanocomposite was separated in the presence of a magnetic stirring bar; the reaction mixture became clear and the crude product was recrystallized from ethanol to give the pure product. The pure products were characterized by conventional spectroscopic methods. Physical and spectral data for selected compound are represented below.

2.7.1. 7-Amino-5-(2-nitrophenyl)-4-Oxo-2-Thioxo-1,3,4,5-Tetrahydro-2H-Pyrano[2,3-*d*]pyrimidine-6-Carbonitrile (8e)

Mp = 242–246 °C; IR (KBr) ν_{max} /cm⁻¹: 3426, 3062, 2197, 1675, 1573, 1518, 1349; ¹H NMR (400 MHz, DMSO-*d*₆):

Table I. Structural parameters of the synthesized Fe_3O_4 @Ph-PMO, and Fe_3O_4 @Ph-PMO-NaHSO₄.

	S_{BET} (m ² · g ⁻¹)	V (cm ³ · g)
Fe_3O_4 @Ph-PMO	357.83	0.5154
Fe_3O_4 @Ph-PMO-NaHSO ₄	163.5	0.3093

Notes: S_{BET} : Specific surface area; V: Total pore volume at relative pressure 0.99.

d (ppm) 5.06 (*s*, 1H), 7.34 (*s*, 2H), 7.48 (*dt*, $J_1 = 7.6$ Hz, $J_2 = 1.6$ Hz, 1H), 7.54 (*dd*, $J_1 = 8$ Hz, $J_2 = 1.2$ Hz, 1H), 7.67 (*dt*, $J_1 = 7.6$ Hz, $J_2 = 1.2$ Hz, 1H), 7.86 (*dd*, $J_1 = 8$ Hz, $J_2 = 1.2$ Hz, 1H), 12.43 (NH, *s*, 1H), 13.67 (NH, *s*, 1H); ¹³C NMR (100 MHz, DMSO-*d*₆): *d* (ppm) 30.7, 56.9, 93.4, 119.0, 124.2, 128.6, 131.5, 133.9, 138.0, 149.7, 152.1, 158.6, 160.7, 174.4.

3. RESULTS AND DISCUSSION

3.1. FT-IR Analysis

Figure 2 shows the FT-IR spectra of the synthesized Fe_3O_4 @Ph-PMO (before and after removal of the template) and Fe_3O_4 @Ph-PMO-NaHSO₄ MNPs, respectively. Before removal of the template (Fig. 2(a)), the FT-IR spectra showed high-intensity peaks for the CH₂ stretching modes located at ~2870 and 2970 cm⁻¹ (symmetric and asymmetric), as well as for the CH₂ bending mode at ~1473 cm⁻¹. These peaks are related to the surfactant tail and their intensities represent to the surfactant concentration. The absence of CH₂ peaks in Figure 2(b), confirms the surfactant removal. Two intense bands at 525 and 1648 cm⁻¹ are attributed to the Si–C and asymmetric phenylene (C=C) stretching modes, respectively. The peaks at 1159 and 2891 cm⁻¹ are attributed to the bridging phenyl C–H vibration and stretching, respectively. The sharp band at 1075 cm⁻¹ from Si–O stretching confirms the formation of siloxane bonds. The band at 3435 cm⁻¹ is from the Si–OH groups. Fe_3O_4 usually presents bands at ~570 and 430 cm⁻¹, due to the Fe–O vibrations in tetrahedral and octahedral sites, respectively. The sulfonic acid bonds can be observed at ~1200–1250, 1010–1100 and 650 cm⁻¹, which are attributed to the O=S=O

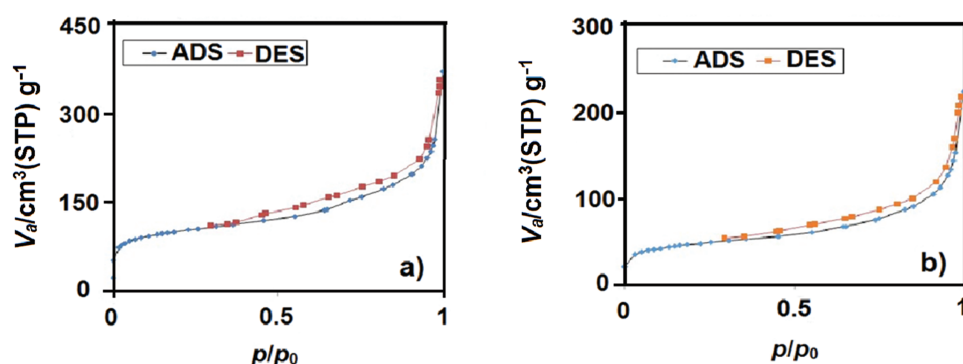


Figure 4. N₂ adsorption–desorption of Fe_3O_4 @Ph-PMO (a), and Fe_3O_4 @Ph-PMO-NaHSO₄ (b).

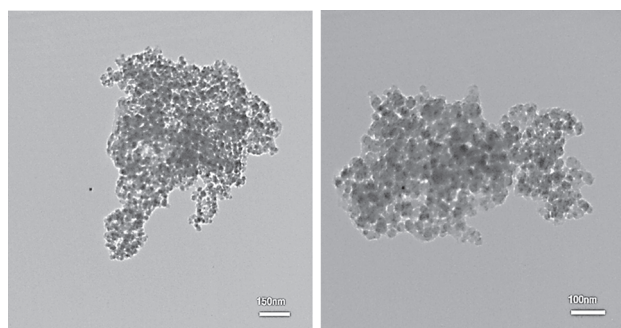


Figure 5. The TEM image of $\text{Fe}_3\text{O}_4@\text{Ph-PMO-NaHSO}_4$.

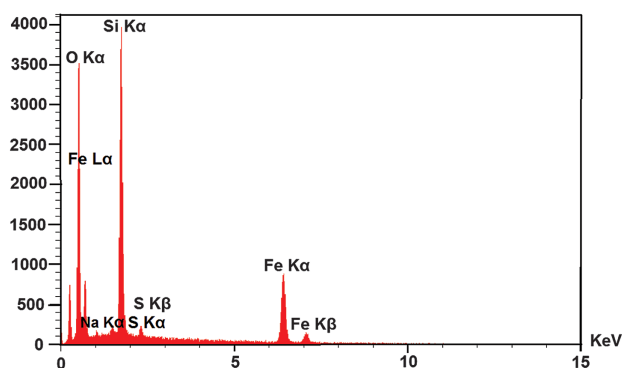


Figure 6. EDX analysis of $\text{Fe}_3\text{O}_4@\text{Ph-PMO-NaHSO}_4$.

asymmetric and symmetric stretching vibrations and S–O stretching vibration of SO_3H groups, respectively. However, in the FT-IR spectra of the synthesized nanoparticles, such bands could not be observed because they are probably overlapped by the bands of SiO_2 . On the other hand, the band at $\sim 3360\text{ cm}^{-1}$ became much broader. The broad peak at $3000\text{--}3500\text{ cm}^{-1}$ is correlated to OH groups of NaHSO_4 and Si–OH groups.

Table II. Optimization of the amount of the catalyst, temperature and solvent in the synthesis of tetrahydrobenzo[*b*]pyran derivative of 4-chlorobenzaldehyde.

Entry	Amount of catalyst (g)	Solvent	Temp. (°C)	Time (min)	Conversion (Yield %) ^a
1	0.02	CH_2Cl_2	r.t.	90	Trace
2	0.02	CH_2Cl_2	Reflux	90	Trace
3	0.02	CH_3CN	r.t.	90	Trace
4	0.02	CH_3CN	Reflux	90	Trace
5	0.02	H_2O	r.t.	90	Not completed
6	0.02	H_2O	80	90	100(80)
7	0.02	$\text{C}_2\text{H}_5\text{OH}$	80	24	100(90)
8	0.02	$\text{C}_2\text{H}_5\text{OH}:\text{H}_2\text{O}$ (1:1)	80	10	100(98)
9	0.01	$\text{C}_2\text{H}_5\text{OH}:\text{H}_2\text{O}$ (1:1)	80	36	100(90)
10	0.02	–	80	25	100(80)
11	0.03	$\text{C}_2\text{H}_5\text{OH}:\text{H}_2\text{O}$ (1:1)	80	20	100(90)

Note: ^aIsolated yields.

Table III. Optimization of the amounts of the catalyst, temperature and solvent in the synthesis of pyrano[2,3-*d*]pyrimidinone derivative of 4-chlorobenzaldehyde.

Entry	Amount of catalyst (g)	Solvent	Temp. (°C)	Time (min)	Conversion (Yield %) ^a
1	0.02	CH_2Cl_2	r.t.	120	Trace
2	0.02	CH_2Cl_2	Reflux	120	Trace
3	0.02	CH_3CN	r.t.	120	Trace
4	0.02	CH_3CN	Reflux	120	Trace
5	0.02	$\text{C}_2\text{H}_5\text{OH}$	r.t.	120	Trace
6	0.02	$\text{C}_2\text{H}_5\text{OH}$	Reflux	120	Not completed
7	0.02	–	80	120	100(90)
8	0.02	H_2O	80	16	100(90)
9	0.03	H_2O	80	8	100(95)
10	0.01	$\text{C}_2\text{H}_5\text{OH}:\text{H}_2\text{O}$ (1:1)	80	20	100(80)
11	–	H_2O	80	120	Trace

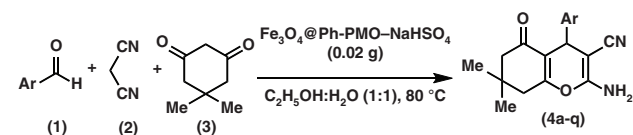
Note: ^aIsolated yields.

3.2. X-ray Diffraction (XRD) Analysis

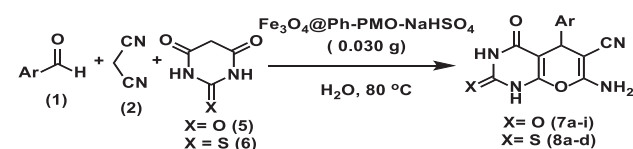
Figure 3 shows the powder X-ray diffraction (XRD) pattern of the synthesized $\text{Fe}_3\text{O}_4@\text{Ph-PMO}$. The peak at 2 theta near 0.9 is related to (d100) hexagonal structures.³⁸ The peaks at $10 < 2\theta < 80$ from $\text{Fe}_3\text{O}_4@\text{Ph-PMO}$ could be confirmed the presence of MNPs. The MNPs indicated peaks with 2 theta at 30.06° , 35.67° , 43.47° , 53.83° , 57.36° and 62.96° which is quite identical to pure magnetite and matched well with the XRD pattern of the standard Fe_3O_4 from Joint Committee on Powder Diffraction Standards (JCPDS No. 19-692).⁴⁰ The XRD measurements of $\text{Fe}_3\text{O}_4@\text{Ph-PMO}$ was carried out to confirm the presence of magnetic nanoparticles in the cave of the synthesized nanocomposite. The same peaks were observed in both bare and periodic mesoporous coated MNPs, indicating the accurate synthesis of the $\text{Fe}_3\text{O}_4@\text{Ph-PMO}$ MNPs.

3.3. BET Analysis

The results of N_2 adsorption–desorption isotherms of $\text{Fe}_3\text{O}_4@\text{Ph-PMO}$ and $\text{Fe}_3\text{O}_4@\text{Ph-PMO-NaHSO}_4$ were



Scheme 1. Synthesis of tetrahydrobenzo[*b*]pyran derivatives catalyzed by $\text{Fe}_3\text{O}_4@\text{Ph-PMO-NaHSO}_4$ in aqueous ethanol (1:1) under thermal condition.



Scheme 2. Synthesis of pyrano[2,3-*d*]pyrimidinone derivatives catalyzed by $\text{Fe}_3\text{O}_4@\text{Ph-PMO-NaHSO}_4$ in water under thermal conditions.

Table IV. Preparation of tetrahydrobenzo[*b*]pyran and pyrano[2,3-*d*]-pyrimidinone derivatives by using Fe₃O₄@Ph-PMO-NaHSO₄ as the catalyst.

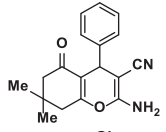
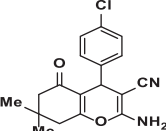
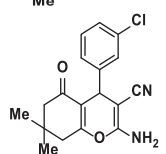
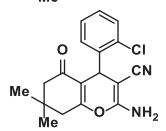
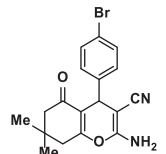
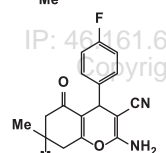
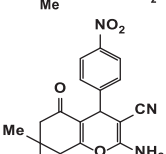
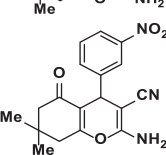
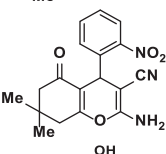
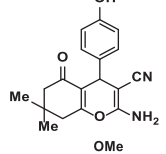
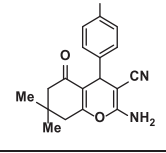
Entry	Aldehyde	Product	Time (min)	Yield (%) ^a		M.P. (°C)		Ref.
						Found	Reported	
1	C ₆ H ₅ CHO		4a	9	95	227–229	227–229	[41]
2	4-ClC ₆ H ₄ CHO		4b	12	98	211–212	210–212	[42]
3	3-ClC ₆ H ₄ CHO		4c	15	93	234–236	235–237	[42]
4	2-ClC ₆ H ₄ CHO		4d	15	95	219–220	218–220	[21]
5	4-BrC ₆ H ₄ CHO		4e	9	97	204–206	203–205	[21]
6	4-FC ₆ H ₄ CHO		4f	10	90	171–174	176–178	[42]
7	4-NO ₂ C ₆ H ₄ CHO		4g	8	95	179–180	177–178	[20]
8	3-NO ₂ C ₆ H ₄ CHO		4h	6	90	211–213	212–214	[21]
9	2-NO ₂ C ₆ H ₄ CHO		4i	8	90	213–217	215–217	[21]
10	4-OHC ₆ H ₄ CHO		4j	35	93	202–205	204–205	[20]
11	4-MeOC ₆ H ₄ CHO		4k	39	90	200–203	199–201	[21]

Table IV. Continued.

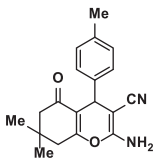
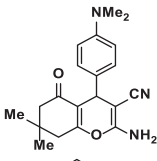
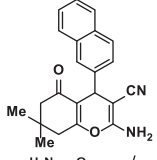
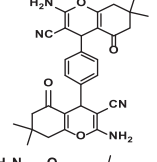
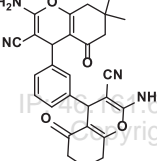
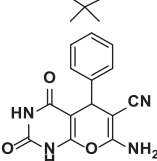
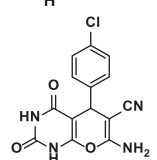
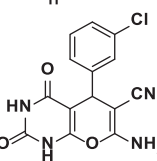
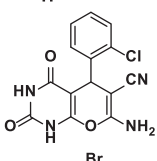
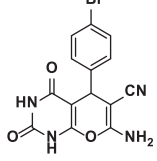
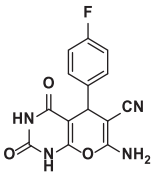
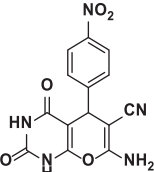
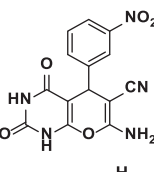
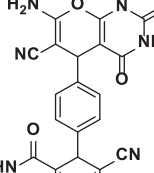
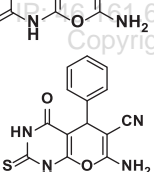
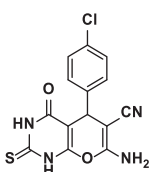
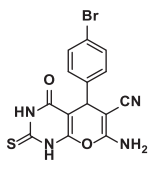
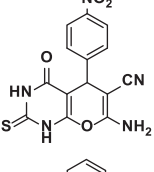
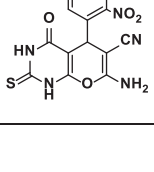
Entry	Aldehyde	Product	Time (min)	Yield (%) ^a		M.P. (°C)		Ref.
						Found	Reported	
12	4-MeC ₆ H ₄ CHO		4m	20	90	211–214	214–216	[23]
13	4-NMe ₂ C ₆ H ₄ CHO		4n	35	85	199–203	198–200	[45]
14	2-Naphthaldehyde		4o	45	92	255–257	258–260	[43]
15	4-CHOC ₆ H ₄ CHO		4p	20	90	264–266	266–268	[44]
16	3-CHOC ₆ H ₄ CHO		4q	25	85	243–244	243–244	[44]
17	C ₆ H ₅ CHO		7a	30	90	214–216	215–217	[35]
18	4-ClC ₆ H ₄ CHO		7b	8	95	238–240	242–243	[35]
19	3-ClC ₆ H ₄ CHO		7c	14	93	238–240	240–241	[34]
20	2-ClC ₆ H ₄ CHO		7d	4	95	212–213	212–214	[34]
21	4-BrC ₆ H ₄ CHO		7e	10	95	227–230	230–231	[30]

Table IV. Continued.

Entry	Aldehyde	Product	Time (min)	Yield (%) ^a		M.P. (°C)		Ref.
						Found	Reported	
22	4-FC ₆ H ₄ CHO		7f	20	80	264–266	268–270	[36]
23	4-NO ₂ C ₆ H ₄ CHO		7g	4	85	237–239	238–240	[36]
24	3-NO ₂ C ₆ H ₄ CHO		7h	25	85	268–270	267–269	[46]
25	4-CHOC ₆ H ₄ CHO		7i	40	90	>300	335–337	[45]
26	C ₆ H ₅ CHO		8a	20	85	220–224	224–225	[35]
27	4-ClC ₆ H ₄ CHO		8b	30	90	>300	>300	[35]
28	4-BrC ₆ H ₄ CHO		8c	35	85	235(dec.) ^b	236(dec.)	[30]
29	4-NO ₂ C ₆ H ₄ CHO		8d	40	83	233–235	235–236	[30]
30	2-NO ₂ C ₆ H ₄ CHO		8e	42	84	242–245	242–246	[49]

Notes: ^aIsolated yields. ^bDecomposition.

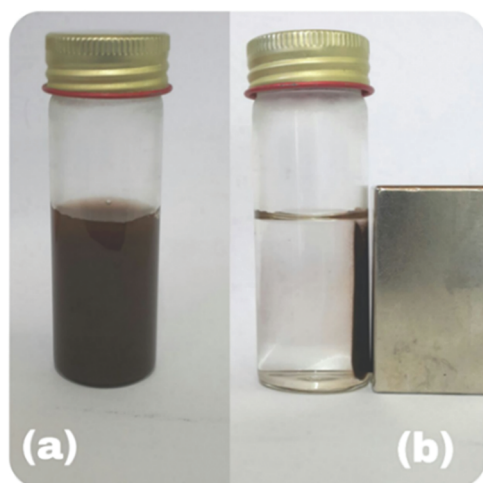


Figure 7. Photographs of an aqueous suspension of Fe_3O_4 @Ph-PMO-NaHSO₄ before (a) and after (b) magnetic capture.

shown in Figure 4. From N_2 adsorption–desorption analysis of samples, a type IV BET isotherm for both samples was obtained, as shown in Figure 4, which is attributed to mesoporous structures.³⁸ The Brunauer-Emmet-Teller (BET) surface areas and total pore volume of Fe_3O_4 @Ph-PMO were $357.83 \text{ m}^2 \cdot \text{g}^{-1}$ and $0.5154 \text{ cm}^3 \cdot \text{g}^{-1}$, respectively. The BET surface area and total pore volume of Fe_3O_4 @Ph-PMO-NaHSO₄ decreased which proves the adsorption of NaHSO₄ on the surface and successful synthesis of the nanocatalyst. Table I summarizes the structural parameters obtained from N_2 adsorption–desorption.

3.4. TEM Analysis

Figure 5 shows TEM image of the synthesized Fe_3O_4 @Ph-PMO-NaHSO₄. The TEM image revealed that all samples were spherical-like particles. Based on the TEM images, analysis of the Fe_3O_4 @Ph-PMO-NaHSO₄ surface morphology demonstrated that the aggregation of the particles is uniform and the size of them is up to 15 nm.

3.5. EDX Analysis

The energy-dispersive Xray analysis (EDX) analysis (Fig. 6) of the catalyst showed the presence of Fe, Si, Na, S, O, and C elements in the expected nanocatalyst.

3.6. H^+ Content Determination

The amount of exchangeable H^+ was determined by neutralization titration. For this purpose, 0.02 g Fe_3O_4 @Ph-PMO-NaHSO₄ was dispersed in 10 mL of NaCl solution (0.1 M) and stirred for 30 minutes then the mixture was titrated with NaOH (0.02 M) in the presence of phenolphthalein as indicator. The amounts of acidic protons were found to be $0.8 \text{ mmol} \cdot \text{g}^{-1}$. This result confirms the synthesis of nanocatalyst and acting it as a solid acid catalyst.

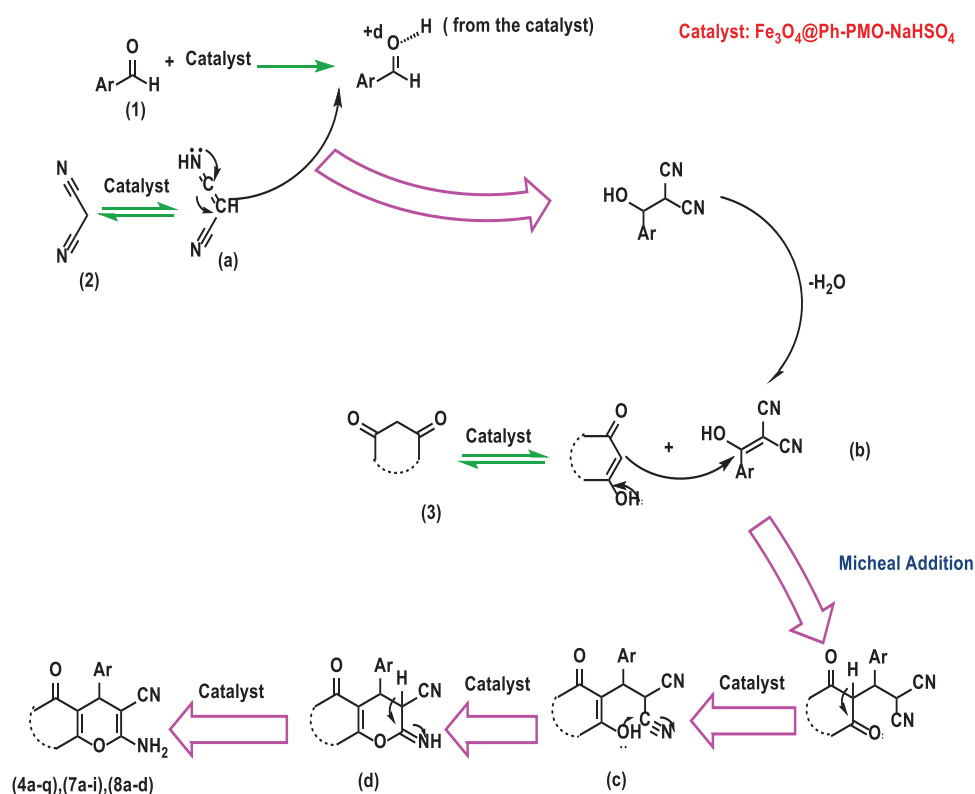
3.7. Catalytic Activity

The above mentioned structural analysis results directed us to assume that Fe_3O_4 @Ph-PMO-NaHSO₄ may be able to promote the organic transformations which need the acidic catalysts to speed-up. In order to confirm this assumption the promoting ability of this reagent was studied in the preparation of tetrahydrobenzo[*b*]pyran and pyrano [2,3-*d*]pyrimidinone derivatives. To prepare these compounds, the reaction of 4-chlorobenzaldehyde (1.0 mmol), malononitrile (1.0 mmol), and dimedone (1.0 mmol) or barbituric acid (1.0 mmol) was selected as a model system. Then the effect of the amounts of the catalyst, temperature, and solvent for the more efficient conditions was investigated and the obtained results were arranged in Tables II and III. After the selection of the best conditions, as indicated in Schemes 1 and 2, a wide range of aromatic aldehydes were subjected to react with malononitrile and 1,3-cyclohexanedione or barbituric acid in the presence of Fe_3O_4 @Ph-PMO-NaHSO₄ to generate the requested products and the results were summarized in Table IV. Also, the reactions were checked by aliphatic aldehydes that lead to a mixture of unidentified products. So the method is not useful for these types of compounds. It is important

Table V. Catalytic activity and reaction conditions comparison of Fe_3O_4 @Ph-PMO-NaHSO₄ with other reported catalysts in the synthesis of 4b and 7e products.

Entry	Catalyst	Amount	Condition	Time (min)	Yield (%)	TOF (s^{-1}) ^c	Ref.
1	$\text{KAl}(\text{SO}_4)_2 \cdot 12\text{H}_2\text{O}$ (alum)	(0.1 mol)	$\text{H}_2\text{O}/80^\circ\text{C}$	40	93	0.0008	[32]
2	Tetrabutylammonium bromide	(0.1 mol)	$\text{C}_2\text{H}_5\text{OH}/\text{reflux}$	30	95	0.0016	[42]
3	Na_2SeO_4	0.1 g	$\text{H}_2\text{O}: \text{C}_2\text{H}_5\text{OH} (1:1)/\text{reflux}$	180	90	0.083	[47]
4	<i>p</i> -Dodecylbenzenesulfonic acid ^a	$(4 \times 10^{-4} \text{ mol})$	$\text{H}_2\text{O}/\text{reflux}$	240	69	0.037	[23]
5	$\text{Fe}_3\text{O}_4\text{-SiO}_2\text{-Met}$	0.03 g	$\text{H}_2\text{O}: \text{C}_2\text{H}_5\text{OH} (1:1)/\text{reflux}$	60	86	0.796	[48]
6	Fe_3O_4 @Ph-PMO-NaHSO ₄	0.02 g	$\text{H}_2\text{O}: \text{C}_2\text{H}_5\text{OH} (1:1)/\text{reflux}$	12	98	6.8	[This work]
7	Diammonium hydrogen phosphate ^b	(0.1 mol)	$\text{H}_2\text{O}: \text{C}_2\text{H}_5\text{OH} (1:1)/\text{r.t.}$	120	81	0.0009	[30]
8	<i>L</i> -Proline ^b	(0.05 mol)	$\text{H}_2\text{O}: \text{C}_2\text{H}_5\text{OH} (1:1)/\text{r.t.}$	90	75	0.0024	[31]
9	$\text{KAl}(\text{SO}_4)_2 \cdot 12\text{H}_2\text{O}$ (alum)	(0.1 mol)	$\text{H}_2\text{O}/80^\circ\text{C}$	30	85	0.0009	[32]
10	Tetrabutylammonium bromide	(0.1 mol)	$\text{H}_2\text{O}/\text{reflux}$	30	95	0.0016	[21]
11	SBA-Pr-SO ₃ H	0.02 g	Neat/ 140°C	20	61	2.541	[29]
12	Fe_3O_4 @Ph-PMO-NaHSO ₄	0.03 g	$\text{H}_2\text{O}/80^\circ\text{C}$	10	95	5.278	[This work]

Notes: ^aAldehyde (1 mmol), dimedone (1 mmol) and malononitrile (1.1 mmol) were used in this method. ^bIn this method, ratio of aldehyde (mmol): barbituric acid (mmol): malononitrile (mmol): is 1:1:1.2. ^cThe amounts of catalysts in TOF were calculated in term of gram of catalysts for all mentioned catalysts in the table.



Scheme 3. Plausible mechanism for the preparation of tetrahydrobenzo[*b*]pyran (4) and pyrano [2,3-*d*]pyrimidinone (7 and 8) derivatives.

to note that the superparamagnetic property of the synthesized nanocatalyst made the separation and reuse of this catalyst very easy. Figure 7 shows the separation of this nanocatalyst from its aqueous dispersion within a few minutes.

To demonstrate the worthiness of the prepared catalyst, the results obtained from the synthesis of 2-amino-4-(4-chlorophenyl)-7,7-dimethyl-5-oxo-5,6,7,8-tetrahydro-4*H*-chromene-3-carbonitrile (4b) (Entry 2, Table IV) and 7-amino-5-(4-bromophenyl)-2,4-dioxo-1,3,4,5-tetrahydro-2*H*-pyrano[2,3-*d*]pyrimidine-6-carbonitrile (7e) (Entry 21, Table IV) using this method is compared with the selected catalysts in Table V. This comparison shows the effectiveness of the heterogeneous catalyst $\text{Fe}_3\text{O}_4@\text{Ph-PMO-NaHSO}_4$ in increasing of the rate and yield of the reaction. The turnover frequency (TOF) was calculated and the higher amount of it displays the better performance of the prepared catalyst in comparison with others as shown in Table V. On the other hand, the catalyst can be easily separated using an external magnetic field, and the reaction proceeds under mild conditions.

A suggested mechanism for the studied reactions is shown in Scheme 3. According to this mechanism, the $\text{Fe}_3\text{O}_4@\text{Ph-PMO-NaHSO}_4$ catalyst activates the carbonyl of the aromatic aldehyde to produce the intermediate (b). In continue, this intermediate reacts with beta-diketone to give the intermediate (c). This intermediate undergoes

cyclo condensation and dehydration to produce the corresponding product.

3.8. Reusability of the Catalyst

The recovery ability of $\text{Fe}_3\text{O}_4@\text{Ph-PMO-NaHSO}_4$ was measured in the synthesis of 7-amino-6-cyano-5-(4-chlorophenyl)-5*H*-pyrano[2,3-*d*]pyrimidinone (7b) and in the synthesis of 2-amino-4-(4-chlorophenyl)-7,7-dimethyl-5-oxo-5,6,7,8 tetrahydro-4*H* chromene-3-carbonitrile (4b) under optimized reaction conditions. After completion of the reaction and separation of the catalyst from the reaction

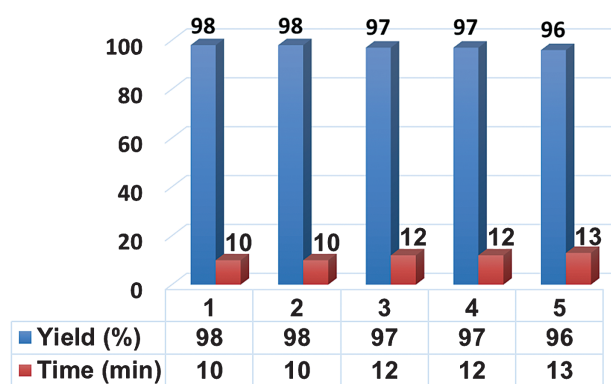


Figure 8. Reusability of $\text{Fe}_3\text{O}_4@\text{Ph-PMO-NaHSO}_4$ in the synthesis of 2-amino-4-(4-chlorophenyl)-7,7-dimethyl-5-oxo-5,6,7,8-tetrahydro-4*H*-chromene-3-carbonitrile (4b).

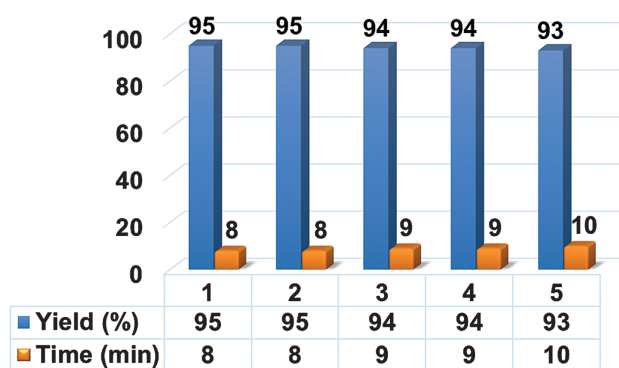


Figure 9. Reusability of $\text{Fe}_3\text{O}_4\text{@Ph-PMO-NaHSO}_4$ in the synthesis of 7-amino-5-(4-chlorophenyl)-2,4-dioxo-1,3,4,5-tetrahydro-2H-pyrano[2,3-d]pyrimidine-6-carbonitrile (7b).

mixture, the catalyst was washed with ethanol, dried in air, and reused with the least change in the reaction time and yield even after five cycles of the synthesis of the product (Figs. 8 and 9). The amount of the acidic protons for both fresh and the recycled catalyst after fifth run was measured by the neutralization titration as mentioned before. According to this, the amount of acidic protons was changed from 0.8 mmol/g for fresh catalyst to 0.6 mmol/g for recycled catalyst, whereas this factor was 0.2 mmol/g for $\text{Fe}_3\text{O}_4\text{@Ph-PMO}$, which showed that although washing with water/ethanol leached out a small amount of NaHSO_4 , due to its highly solubility, the products were obtained in least change in reaction times and yields.

4. CONCLUSION

In conclusion, $\text{Fe}_3\text{O}_4\text{@Ph-PMO-NaHSO}_4$ as a new nanocatalyst was successfully synthesized and utilized as an efficient catalyst for the preparation of tetrahydrobenzo[b]pyran and pyrano[2,3-d]pyrimidinone derivatives under mild conditions. This catalyst is thermally stable, green, recyclable, inexpensive and easy to prepare. In addition, it can be easily separated from the reaction mixture and recovered up to five times without any significant influence on its activity or the reaction yield. The operational simplicity, high yields, and easy work-up procedure associated with this catalytic process give it advantages over the other methods.

Acknowledgments: We are thankful to the Research Council of the University of Guilan for the partial support of this research.

References and Notes

- S. S. Park, M. S. Moorthy, and C. Ha, *Korean J. Chem. Eng.* 31, 1707 (2014).
- M. Sharifi, D. Wallacher, and M. Wark, *Beilstein J. Nanotechnol.* 3, 428 (2012).
- C. W. Jones, K. Tsuji, and M. E. Davis, *Nature* 393, 52 (1998).
- F. Hoffmann, M. Cornelius, J. Morell, and M. Fröba, *Angew. Chem. Int. Ed.* 45, 3216 (2006).
- D. Margolese, J. A. Melero, S. C. Christiansen, B. F. Chemelka, and G. D. Stucky, *Chem. Mater.* 12, 2448 (2000).
- L. Mercier and T. J. Pinnavaia, *Chem. Mater.* 12, 188 (2000).
- S. Inagaki, S. Guan, Y. Fukushima, T. Ohsuna, and O. Terasaki, *J. Am. Chem. Soc.* 121, 9611 (1999).
- B. J. Melde, B. T. Holland, C. F. Blandford, and A. Stein, *Chem. Mater.* 11, 3302 (1999).
- T. Asefa, M. J. MacLachlan, N. Coombs, and G. A. Ozin, *Nature* 402, 867 (1999).
- F. Goethals, B. Meeus, A. Verberckmoes, P. Van der Voort, and I. Van Driessche, *J. Mater. Chem.* 20, 1709 (2010).
- Q. H. Yang, J. Liu, H. Zhong, and P. Y. Wang, *J. Inorg. Mater.* 24, 641 (2009).
- N. Mizoshita, T. Tani, and S. Inagaki, *Chem. Soc. Rev.* 40, 789 (2011).
- W. O. Foye, T. L. Lemke, and D. A. Williams, *Principi di Chimica Farmaceutica*, edited by Piccin-Nuova Libreria, Padua, Italy (1991), p. 416.
- L. L. Andreani and E. Lepi, *Bull. Chim. Farm.* 99, 583 (1960).
- O. Bruno, S. Schenone, A. Ranise, E. Barocell, M. Chiavarini, V. Ballabeni, and S. Bertoni, *Arzneim. Forsch.* 50, 140 (2000).
- E. M. Griva, S. Lee, C. W. Siyal, D. S. Duch, and C. A. Nichol, *J. Med. Chem.* 23, 327 (1980).
- G. L. Anderson, J. L. Shim, and A. D. Broom, *J. Org. Chem.* 41, 1095 (1976).
- M. M. Ghorab and A. Y. Hassan, *Phosphorus, Sulfur, Silicon Related Elem.* 141, 251 (1998).
- D. Heber, C. Heers, and U. Ravens, *Pharmazie* 48, 537 (1993).
- X. Zh. Lian, Y. Huang, Y. Q. Li, and W. J. Zheng, *Monatsh. Chem.* 139, 129 (2008).
- A. Mobinikhaledi and M. A. Bodaghi Fard, *Acta Chim. Slov.* 57, 931 (2010).
- J. Azizian, A. Shameli, S. Balalaie, M. M. Ghanbari, Sh. Zomorodbakhsh, M. Entezari, S. Bagheri, and Gh. Fakhrpour, *Orient. J. Chem.* 28, 327 (2012).
- E. Sheikhsosseini, D. Ghazanfari, and V. Nezamabadi, *Iran. J. Catal.* 3, 197 (2013).
- J. Albadi, M. Fadaeian, and F. A. Balout-Bangan, *Iran. J. Org. Chem.* 5, 1089 (2013).
- M. G. Dekamin, M. Eslami, and A. Maleki, *Tetrahedron.* 69, 1074 (2013).
- B. Maleki and S. Sedigh Ashrafi, *RSC Adv.* 4, 42873 (2014).
- B. Maleki, N. Nasiri, R. Tayebbe, A. Khojastehnezhad, and H. A. Akhlaghi, *RSC Adv.* 6, 79128 (2016).
- B. Maleki, M. Baghayeri, S. Ayazi Jannat Abadi, R. Tayebbe, and A. Khojastehnezhad, *RSC Adv.* 6, 96644 (2016).
- B. Maleki, H. Eshghi, M. Barghamadi, N. Nasiri, A. Khojastehnezhad, S. Sedigh Ashrafi, and O. Pourshiani, *Res. Chem. Intermed.* 42, 3071 (2016).
- J. Balalaie, Sh. Abdolmohammadi, H. R. Bijanzadeh, and A. M. Amani, *Mol. Divers.* 12, 85 (2008).
- M. Bararjanian, S. Balalaie, B. Movassagh, and A. M. Amani, *J. Iran. Chem. Soc.* 6, 436 (2009).
- N. Mobinikhaledi, M. Foroughifar, and M. A. Bodaghi Fard, *Synth. React. Inorg. Metal-Org. Nano-Metal Chem.* 40, 179 (2010).
- Gh. M. Ziarani, S. Faramarzi, Sh. Asadi, A. Badiei, R. Bazl, and M. Amanlou, *DARU J. Pharm. Sci.* 21, 3 (2013).
- B. Sadeghi, M. Bouslik, and M. R. Shishehbore, *J. Iran. Chem. Soc.* 12, 1801 (2015).
- B. Sabour, M. H. Peyrovi, and M. Hajimohammadi, *Res. Chem. Intermed.* 41, 1343 (2015).
- J. Albadi, A. Mansournezhad, and T. Sadeghi, *Res. Chem. Intermed.* 41, 8317 (2015).
- N. Saadatjoo, M. Golshekan, S. Shariati, H. Kefayati, and P. Azizi, *J. Mol. Catal. Chem.* 377, 173 (2013).

38. C. P. Moura, C. B. Vidal, A. L. Barros, L. S. Costa, L. C. G. Vasconcellos, F. S. Dias, and R. F. Nascimento, *J. Colloid Interface Sci.* 363, 626 (2011).
39. M. Golshekan, S. Shariati, and N. Saadatjooa, *RSC Adv.* 4, 16589 (2014).
40. J. H. Jang and H. B. Lim, *Microchem. J.* 94, 148 (2010).
41. N. Hazeri, M. T. Maghsoodlou, F. Mir, M. Kangani, H. Saravani, and E. Molashahi, *Chin. J. Catal.* 35, 391 (2014).
42. S. Gurumurthi, V. Sundari, and R. Valliappan, *J. Chem.* 6, S466 (2009).
43. A. R. Moosavi-Zare, M. A. Zolfigol, O. Khaledian, V. Khakyzadeh, M. D. Farahani, and H. G. Kruger, *New J. Chem.* 38, 2342 (2014).
44. F. Shirini, O. Goli-Jolodar, M. Akbari, and M. Seddighi, *Res. Chem. Intermed.* 42, 4733 (2015).
45. F. Shirini, M. Safarpour Nikoo Langarudi, and N. Daneshvar, *J. Mol. Liq.* 234, 268 (2017).
46. O. Goli-Jolodar, F. Shirini, and M. Seddighi, *J. Iran. Chem. Soc.* 13, 457 (2016).
47. R. Hekmatshoar, S. Majedi, and K. Bakhtiari, *Catal. Commun.* 9, 307 (2008).
48. A. Alizadeh, M. Khodaei, M. Beygzadeh, D. Kordestani, and M. Feyzi, *Bull. Korean Chem. Soc.* 33, 2546 (2012).
49. F. Shirini, M. Safarpour Nikoo Langarudi, and N. Daneshvar, *RSC Adv.* 6, 44630 (2016).

Received: 11 March 2018. Accepted: 22 April 2018.

IP: 46.161.60.137 On: Sun, 17 Mar 2019 02:32:34
Copyright: American Scientific Publishers
Delivered by Ingenta